REVIEW PAPER

The Microfluidic Sensors of Liquids, Gases, and Tissues Based on the CNT or Organic FETs

Received 19th March; accepted 20th April.

Rostyslav Sklyar

Abstract:

A superconducting field effect transistor based transducer (SuFETTr) for the micro- and nanofluidic sensors to measure the electrical currents and mechanical flows has been described. SuFETTr device consists of either CNT or organic FETs with a superconducting property. The flowmeters are based on a common or superconducting induction sensors employing the magnetohydrodynamical and electrogaseodynamical effects. The range of the calculated signals lies in the range of – (5÷5)V, (7÷0)·10[17]/cm3 molecules, (2÷10) pH, and stream speed (10[2]÷10[-3]) m/s, flow (10[1]÷10[-5])m/s and hemoglobin concen-tration of (10[30]÷10[24])molec/mm[3]. The available operating modes have been explained.

Keywords: *magnetohydrodynamical effect, electrogaseodynamical flow, hemoglobinum composition, CNT, SuFET, operating modes*

1. Introduction – Microfluidic sensors and diagnostic systems

The sensor converts information or energy from the measurement quantity into another quantity, especially an electrical quantity. This "intermediate" signal may be processed in some way [1]. There are sensor and transducers for electrical quantities especially for current, voltage and magnetic quantities. A biosensor is a device that incorporates a biologically active layer as the recognition element and converts the physical parameters of the biological interaction into a measurable analytical signal [2]. Thanks to advances in nanotechnology, microelectromechanical systems, molecular diagnostics, and several other technologies, biosensors are now being developed to detect everything from the first chemical signature of cancer to the presence of anthrax.

There are a number of methods and devices for transducing different microfluidic biosignals (MBs) into recordable or measurable information. Electric-field control of physical properties is highly desirable from fundamental and technological viewpoints because it does not introduce any chemical or microscopic structural disorder in the pristine material. This is also the basis of FETs, in which accumulation, depletion, and inversion layers are formed at the interface [3]. Moreover, the complex view on MBs requires further stages of precise processing in order to decode the received or control information.

The growing variety of biosensors can be grouped into two categories: implantable and external. Because external sensors employ widely used contact mechanisms like needles and lasers, this branch has advanced faster than implantables. For this reason a working interface between the living tissue of individual neurons and the inorganic compounds of silicon chips was developed. There also provided the link between ionic channels of the neurons and semiconductor material in a way that neural electrical signals could be passed to the silicon chip. Once there, that signal can be recorded using the chip's transistors. What's more, the neurons can also be stimulated through the capacitors. This is what enables the two-way communications. The project tested the device by stimulating the neurons and recording which ones fired using standard neuroscience techniques while tracking the signals coming from the chip [4].

The recent achievements in nanoelectronics can be regarded as a further step in the progress of MB transduction. They give us the possibility to create the most advanced and universal device on the basis of known micro systems. Such a sensor/transducer is suitable for picking up MBs and transforming it into recognizable information in the form of electric voltage, or a concentration of organic or chemical substances. Moreover, this process can be executed in reverse. Substances and/or voltages influence MBs, thereby controling or creating them (MBs). Also the new fiber-based optical microfluidic detectors are designed for nano-volume sample measurement. The silicon-glass microdetectors were fabricated by use of micromechanical techniques [5].

The advent of semiconductor devices with nanoscale dimensions creates the potential to integrate nanoelectronics and optoelectronic devices with a great variety of biological systems. Moreover, the advances in nanotechnology are opening the way to achieving direct electrical contact of nanoelectronic structures with electrically and electrochemically active subcellular structures-including ion channels, receptors, and transmembrane proteins such as bacteriorhodopsin. Direct electrical interfacing at the biomolecular level opens the possibility of monitoring and controlling critical biological functions and processes in unprecedented ways, and portends a vast array of possibilities such as new classes of prosthetic devices, medical monitoring devices, medical delivery systems, and patient monitoring systems, as well as other applications [6].

A major challenge for the next 510 years is the reproducible placement and seamless interfacing of functionalized nanoscale features and messaging systems within a chip-based device to measure and interpret complex biological processes in real time [7].

Major challenges remain for probing cell biology at the nanometer scale. Because diffusion across the cell cytoplasm of second messenger molecules such as calcium ions occurs on a subsecond time scale, future self-contained, chip-based laboratories must be capable of reading out and interpreting a large array of multiplexed signals in real time. Detecting signals with adequate signal-to-noise ratio is not currently feasible in realtime readouts from sensor arrays that are spatially dense at nanometer length scale.

Sensors and Diagnostic Instruments

Electrical current may be measured by measuring the related magnetic field (MF) by means of the Hall effect or the Faraday effect into optoelectronic devices. The measurand as well as the reference value are often converted into quantities of either the same or different physical nature before they are actually compared with each other [1]. Proceeding from the previously mentioned difficulties, including superconducting element of the sensor/transducer into an electric current could be the solution to the problem. Electronic or ionic currents in conductors or axons respectively, passing through the SuFET's channel induce the output voltage on its gate [8].

The lab-on-a-chip systems use dielectrophoretic forces to direct cell movement within microfluidic networks and impedance spectroscopy for label-free inflow characterization of living cells. The implantable microelectrodes for neural applications are based on thin-film polymer foils with embedded microelectrodes for both recording and stimulation. Applications for these biomedical microdevices will include stem cell research, cancer cell characterization, drug discovery, treatments for neurological disorders, and neuroprosthetic devices [9].

Whereas the sensor element can deliver a weak signal, the transmitted signal should generally have a high signal level, and perhaps suitable values, in order to reach superior units undisturbed and to simplify the following calculations. Therefore, the sensor signal should be generally preprocessed. Thereby several important tasks could be realized, such as signal amplification, scalling, linearization, conversion, and conjunction with other components in a chain, parallel, or closed-loop structure [10].

Typical microfluidic devices consist of microfabricated channels possessing at least one characteristic dimension below a millimeter. At these dimensions, flows tend to be stable and laminar over a wide range of fluid velocities, fluid properties, and channel geometries. The stability, and thus predictability, of these flows arises from the important role of viscous forces at small dimensions, as reflected by a small to moderate Reynolds number. Microfluidic devices often take advantage of these hydrodynamic traits to spatially organize fluid streams bearing chemical reagents, cells, proteins, and other items [11].

At the single-chip level, components are separated into two fundamental categories: passive fluidic components and active electromechanical control structures [12]. Passive components include chemical reactors and channels. Active components are sensors (e.g., flow rate, temperature, pressure) and actuators (e.g., pumps, valves, mixers). Active and passive structures are built separately on different physical layers.

2. The components for cnt based microfluidic sensors

CNT-based nanobiosensors may be used to detect DNA sequences in the body. These instruments detect a very specific piece of DNA that may be related to a particular disease. The use of nanotube-based sensors will avoid problems associated with the current much-larger implantable sensors, which can cause inflammation. The devices can be administered transdermally. CNT chemical sensors for liquids can be used for blood analysis. CNTs can also be used as flow sensors, when the flow of a liquid or bundles induces a voltage in the direction of flow. Flow sensors can also be used for precise measurements of gases utilized by respiratory apparatuses during surgery and automatic calculation of medical treatment fees [13].

Superconducting nanowires are unusual in that they newer show zero resistance, although resistance does exponentially upon cooling [14]. A new class of metallic devices based on DNA molecules is promising due to the self-assembly properties of DNA. As the resistance of the devices is controlled by the spatial profile of superconducting phase within the leads, there is the potential for applications. These include local magnetometry (as is widely done with conventional superconducting quantum interference device (SQUID).

A. Connection of SuFETs with the Microfluidics' Medium

Microdevices with electroplated wire traces were etched with well-defined edges. These devices are implanted in living bodies to connect nerve tissue with electronics to record nerve cell activities or restore lost functions by stimulation of nerve cells. Electroplating of gold meets the requirements for producing neural implants with low-ohmic wire traces, because this technique allows the microfabrication of gold layers with a thickness of several micrometers and lateral dimensions in the same range. Hence the mechanical stability of the electroplated gold is sufficient for chronic implantation of the structures [15]. The implantable microelectrodes for neural applications are based on thin-film polymer foils with embedded microelectrodes for both recording and stimulation [16].

Very efficient attachment mechanisms are those in which patterned surface structures interact with the profile of the substrate. This general trend is quantitatively explained by applying the principles of contact mechanics, according to which splitting up the contact into finer subcontacts increases adhesion. This principle is wide-spread in the design of natural adhesive systems and may also be transferred into practical applications [17].

Recently, strong evidence has been presented that the adhesion of gecko setae is caused by van der Waals interaction, rejecting mechanisms relying on capillary adhesion. Elements of contact mechanics have also been applied to this problem and it was predicted that arrays with smaller setae endings should result in greater adhesive strength. An extensive microscopical study of biological surface devices has been combined with the

theory of contact mechanics based on molecular adhesion.

The creation of a permissive environment for axonal regrowth was described using a synthetic biological nanomaterial that self assembles in vivo, with components that break down into beneficial building blocks and produce no adverse effects on the nerve fibre. This discovery, by reducing or overcoming the first two obstacles and possibly more, allows for the reconnection of disconnected parts of the nerve fibre [18]. Thin films of carbon nanotubes deposited on transparent plastic can serve as a surface on which cells can grow and these nanotube films could potentially serve as an electrical interface between living tissue and prosthetic devices or biomedical instruments. Both cell types were placed on ten-layer-thick "mats" of single-walled carbon nanotubes (SWNTs) deposited on transparent plastic. This enabled to use a microscope to position a tiny electrode next to individual cells and record their responses to electrical pulses transmitted through the SWNTs [19].

Imaging studies show how the shape of domain walls evolve as they move along a ferromagnetic nanowire [20]. Over macroscopic length scales, uniform magnetization is energetically unfavourable and domain walls regions where the magnetization rotates will form. The wires are indented on one edge so that when a domain wall forms and is forced to propagate along the wire length, it becomes pinned at the notch. Multisegmented one-dimensional hybrid structures of carbon nanotubes and metal nanowires were fabricated using the alumina templates [21]. Well-adhered interfaces formed between the carbon nanotubes and the metal nanowires. The hybrid structure reported here results in nanoscale metal contact with carbon nanotube and will provide a solution to problem of using carbon nanotubes in interconnects.

B. The available FET's variants applicable as SuFET

Application of the SuFET's modifications such as CMOSuFET (low Tc) [22] and coplanar SuFET (high Tc) [23] broadens the range of requirements which are being satisfied by the SuFETTr. Low-dimensional semiconductor nanostructures and organic molecules, which offer unique possibilities such as extremely low power dissipation, quantum effects, surface sensitivity and low synthesis cost, could be the building blocks for next-generation electronics [24]. Moreover, an organic superconductivity of carbon molecules, known as bucky balls, which can act as superconductors at relatively warm temperatures, raises hopes for loss-free organic electronics and their practical applications in biosensors, including organic ones.

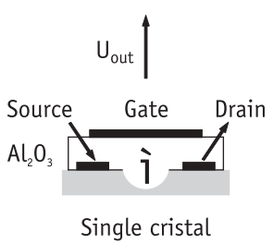

Fig. 1 An organic SuFET device and its electrodes

High densities of electrons and holes have been induced by gate doping in a FET geometry (Fig. 1). At low temperatures, the material turns superconducting with a maximum transition temperature of 117 K in hole-doped $C_{60}/CHBr_3$ [25]. The increased spacing between the C_{60} molecules increases the density of states, and the resulting increase of TC is well documented in alkali metaldoped bulk samples (A_3C_{60}). The observation of gate-induced hole doping of C_{60} resulting in a T_c of 52 K suggests that significantly higher T_cs could be anticipated in suitably "expanded" C_{60} crystals. Indeed, here is reported a raise in T_c to 117 K with such methods.

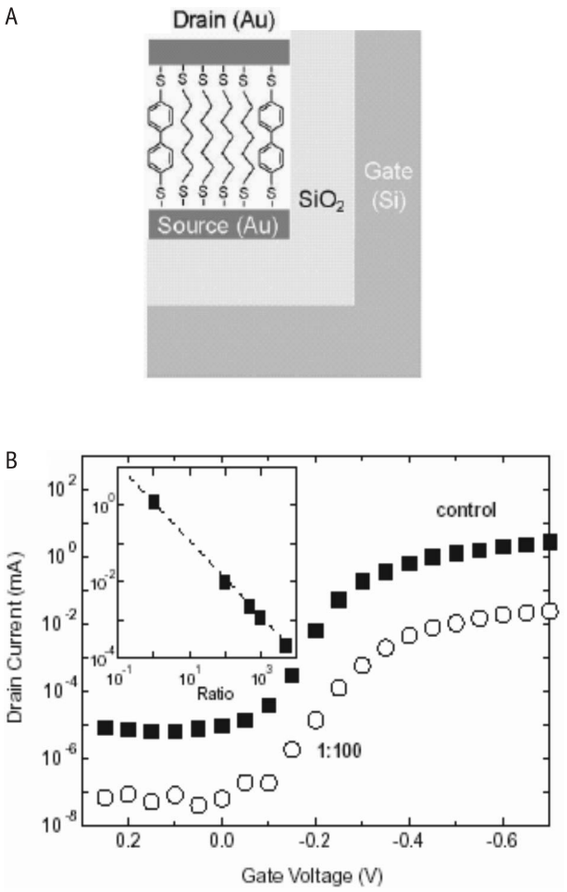

Fig. 2 A - SAMFET structure. A highly doped Si substrate is used as the gate electrode, a thermally grown SiO2 layer acts as gate insulator, the gold source electrode is deposited by thermal evaporation, and the active semiconducting material is a two-component SAM of alkanedithiols mixed with 4,49-biphenyldithiol or 5,59-terthiophenedithiol. The drain contact is defined by shallow angle shadow evaporation of gold. The active region of the device is magnified;

B - Transfer characteristics at room temperature of two SAMFETs (drain-source voltage of 20.5 V). The control corresponds to a "pure" 4,49-biphenyldithiol SAM, whereas the second one is based on a twocomponent SAM (4,49-biphenyldithiol to alkanedithiol ratio is 1:100). The inset shows the current at a gate and drain-source voltage of 20.5 V as a function of the mixture ratio.

A

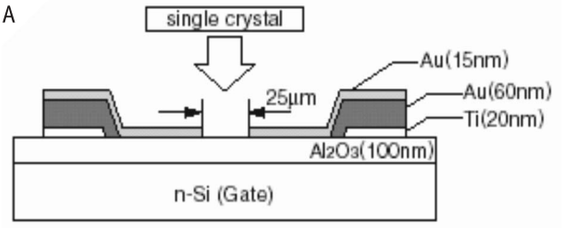

B

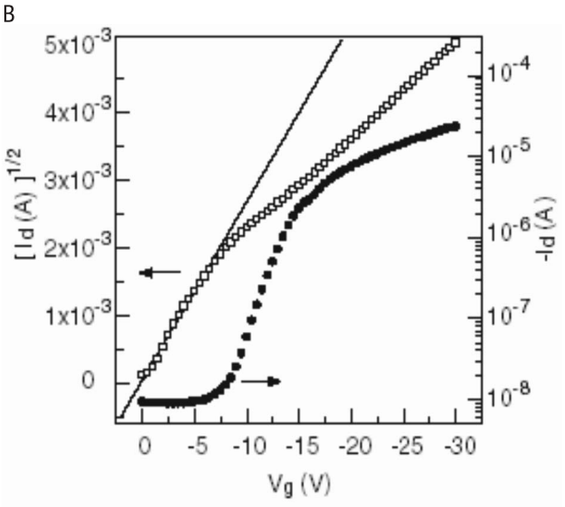

Fig. 3 OFET of organic single crystals with bottom - contact configuration
A - the schematic structure of the fabricated OFET;
B - transfer characteristics of the single crystal FET device at a source - drain voltage Vd of - 30 V.

1. Organic FETs with a superconducting potential

Vertical self-assembled monolayer (SAM) FET (SAMFET) action, i.e., conductance modulation through a third electrode, in devices consisting of only several electrically active molecules has been reported [26]. The channel length of 10 to 20 Å is defined by the thickness of a SAM rather than lithography (Fig. 2). Moreover, the peak conductance at low temperatures is quantized in units of $2e^2/h$, indicating that the conductance of single molecules is modulated.

Organic FETs (OFETs) are of great interest for future electroritic applications due to their flexibility. Up to now, a lot of fabrication processes or device configurations of OFETs have been reported [27]. Most of them were based on thin film technique such as vapor deposition. In general, the thin films for example, amorphous, poly crystalline, polymeric, and so on, consist of grains, and therefore, charge carriers behave as hopping conduction. This decreases the field-effect mobility of devices. Thus, annealing the organic thin films or surface preparations of substrate grows grains, and consequently these devices have few boundaries of grains between source and drain electrodes.

A quite simple and easy fabrication technique of OFETs with single crystals was proposed, and it demonstrated that the OFETs exhibit high mobility and good device characteristics (Fig. 3). The presented technique makes the fabrication of high performance OFETs easy and serves as a potential way to make organic integrated circuits. Also N-channel and ambipolar OFETs with a few tens of nanometer channel length were fabricated and characterized [28].

A

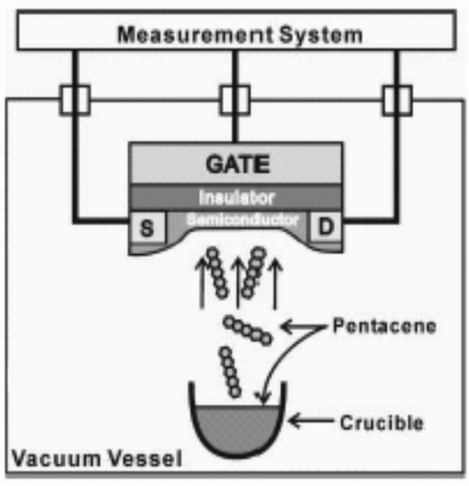

B

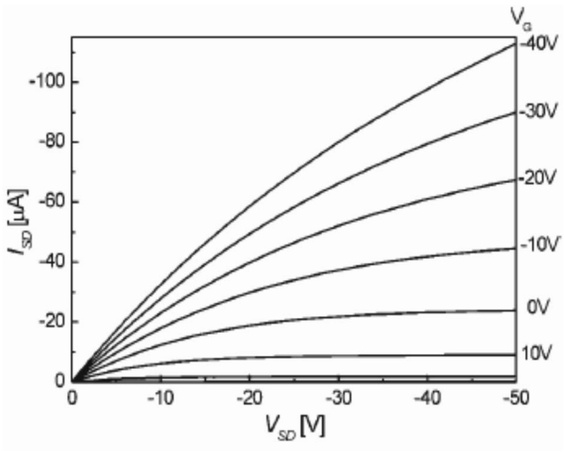

Fig. 4 Thin film (TFT) FET
A - The source - drain current was measured in situ at various gate voltages;
B - shows channel current (ISD) versus voltage (VSD) for the 20 nm thick pentacene TFT FET.

A

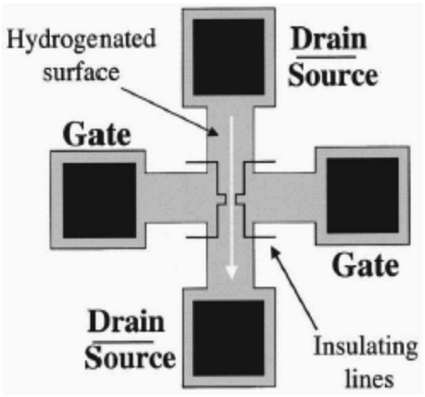

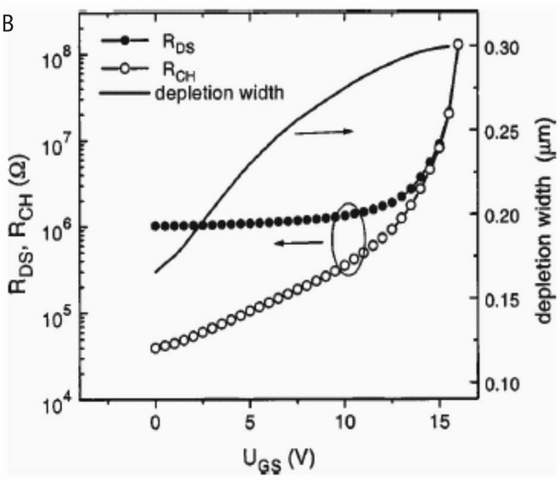

Fig. 5 In-plane gate FET on hydro-genated single-crystal diamond surface
A - Schematic diagram of an in-plaine FET;
B - Drain-source resistance R_{DS}, channel resistance R_{CH}, and depletion region width as a function of the gate voltage V_{GS}.

A simple but powerful method to observe directly the regions in which the carriers are exhausted or injected by electric fields has been proposed [3]. As shown in the Fig. 4, the source (S)-drain (D) current in thin film transistors (TFT) is measured as a function of the film thickness with a bottom-contact configuration.

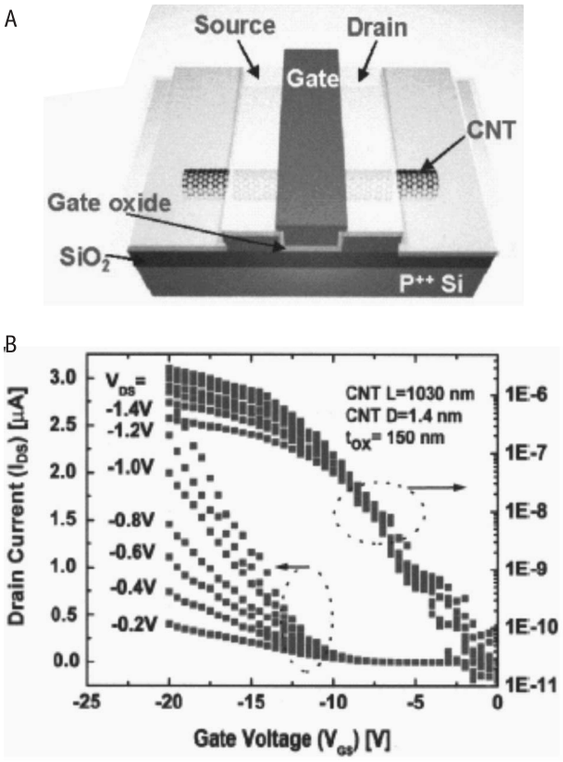

Fig. 6 Schematic representation of top-gated CNTFET
A - The SWCNT played the role of the "channel," while the two metal electrodes functioned as the "source" and "drain" electrodes. The heavily doped silicon wafer itself was used as the "gate" (back-gate);
B - Transfer characteristics of such a CNTFET.

The fabrication and characterization of in-plane gate transistors on hydrogenated single-crystal diamond surfaces have been reported [29]. A wire structure is designed in such a way that the conductance of the channel is modulated by the gate voltage (Fig. 5). The combination of the biocompatibility and tissue equivalence of diamond, as well as the metal-free surface of these in-plane devices, in particular, may open interesting applications for diamond in bioelectronics.

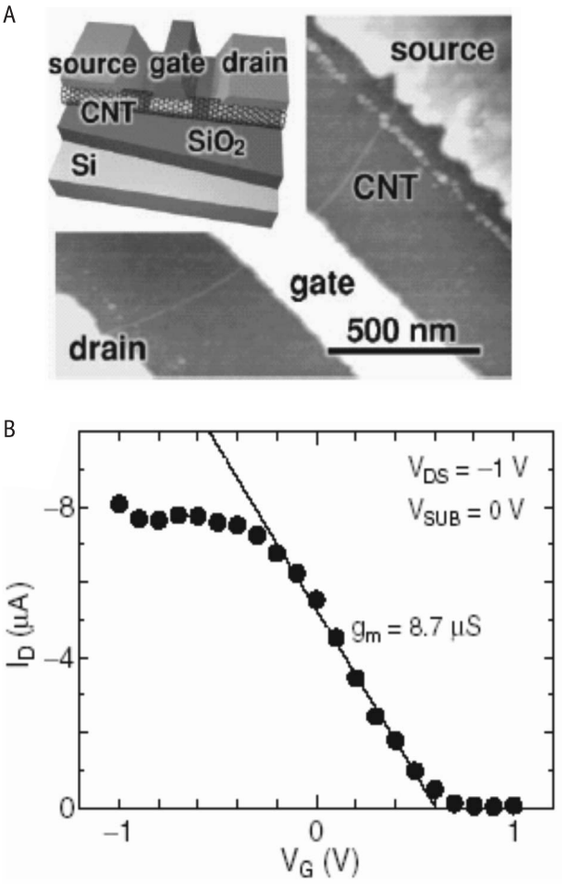

Fig. 7 CNTFETs with CNTs grown by chemical vapor deposition combined with low-resistance ohmic contacts and top gates
A - an AFM image of an individual CNT bridging the 1-mm gap between the source and drain electrodes. The gate electrode (LG 210 nm) is formed on the CNT. Inset: Schematic structure of the CNTFET;
B - CNTFET's channel current IDS as a function of V_{GS} at V_{DS}= -1V.

2. NanoFETs with superconducting CNT channel (nano SuFETs)

The first such devices were fabricated in 1998. The CNT was simply laid on the gold electrodes and was held by weak van der Waals forces. In addition to increasing the gate capacitance, it is essential that each CNT FET is gated independently by its own gate so that complex integrated circuits can be built [30]. The next generation of CNTFETs with top gates was fabricated by dispersing single-walled (SW) CNTs (SWCNTs) on an oxidized wafer (Fig. 6).

The intrinsic transconductance of CNTFETs in which CNTs were grown by chemical vapor deposition was measured at a drain voltage of -1V was 8.7 mS for a CNT with a diameter of 1.5 nm (Fig. 7). Estimated intrinsic transconductance was 20 mS, when parasitic resistance was taken into account. Measured and intrinsic transconductance per unit channel width were 5800 mS/mm and 13000 mS/mm, respectively. This is considerably larger than those for stateof- the-art Si-MOSFETs. This transconductance can be improved drastically by decreasing parasitic resistance and the performance of CNT FETs will advance further by improving the CNT quality and the device structures [31].

The importance of being able to address nanoscale elements in arrays goes beyond the area of nanocomputing and will be critical to the realization of other integrated nanosystems such as chemical/-biological sensors. A regular crossed-nanowire FET (cNW-FET) array (Fig. 8.A) that consists of n-input í and m-output V_{out} n NWs, in which outputs are the active channels of FETs and the inputs function as gate electrodes that turn these output lines on and off [32]. Conductance versus applied NW input gate voltage data (Fig. 8.B) shows that each of the four cNW-FET elements could be turned off with gate voltage of 1V to 2 V, whereas the off-diagonal elements remained unaffected for the same input voltage. When NW are superconducting and, as a result, all cNW-FETs are functioning in SuFET mode, such output voltage V_{out} will show the changes in their conductance.

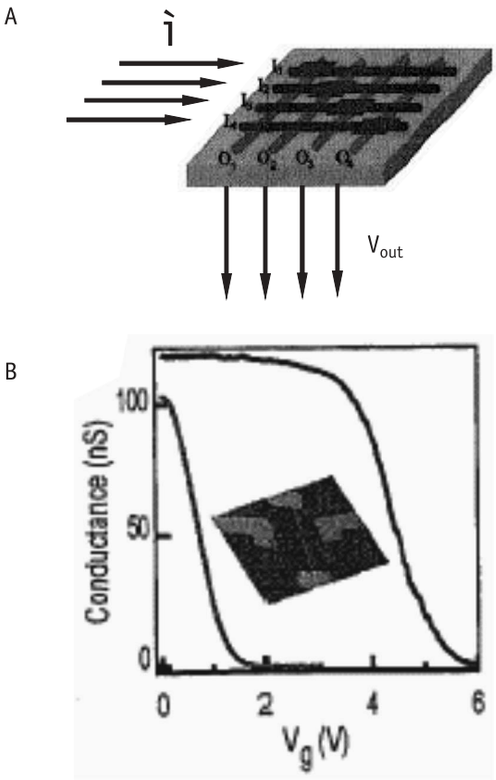

Fig. 8 A 4 by 4 crossed NW-FET array
A - with four horizontal NWs (I1 to I4) as inputs and four vertical NWs (O1 to O4) as signal outputs;
B - conductance versus gate voltage of a single cNW-FET.

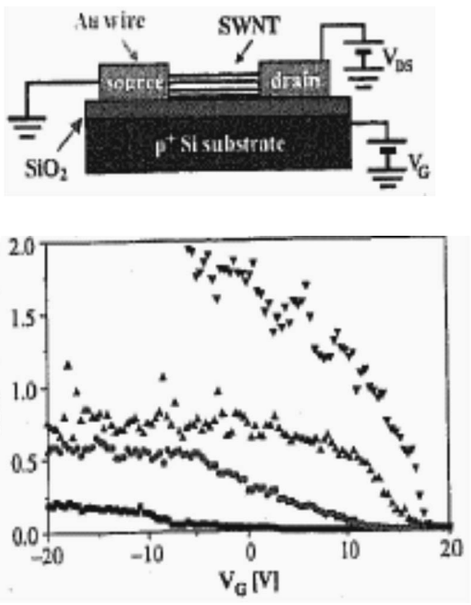

Fig. 9 A self-assembled SWNT-FET
A - schematic representation of the electrical measurement circuit;
B - drain-source current versus gate voltage for different values of drain-source bias.

The realization of a self-assembled SW CNT FET operating at room temperature promotes such strategy as realistic for construction CNT-based electronics (Fig. 9). The assembly process was guided by the information encoded in DNA molecules and homologous genetic recombination [33].

Using a variant of nano patterning, a self-assembling polymer could also create tiny, finger-shaped silicon protrusions sticking up from the underlying substrate [34]. These fingers would constitute the "channel" in a transistor through which electrons flow – but one in which electrons flow vertically instead of across a chip, as in today's devices (Fig. 10). The gate to turn the transistor off and on could encircle the silicon finger. The geometry might prevent electrons from "tunneling", or leaking, through the channel when the transistor is in the off state, a constant threat when feature sizes become very small.

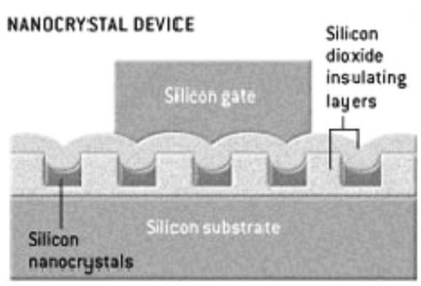

Fig. 10 Self-assembled nanocrystal FET
A layer of self-assembled silicon nanocrystals is inserted into an otherwise standard device.

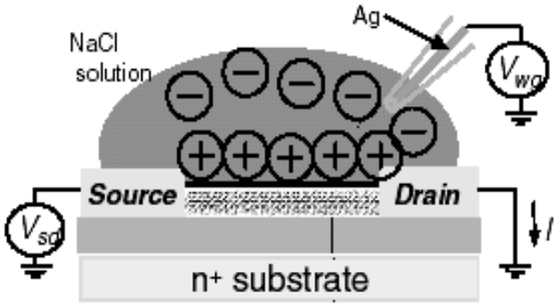

Fig. 11 Schematic of the electrolyte gate measurement
A water-gate voltage voltage Vwg applied to a silver wire in the pipette is used to establish the electrochemical potential in the electrolyte relative to the device. For -0.9V < V_{wg} < 0.9 V, the leakage current between the water and the Au electrodes/SWNT was negligible (less than 1 nA); the electrolyte then functions as a well-insulated liquid gate.

The excellent device characteristics of SW CNT transistors in salty water also indicate that they may be ideal for biosensing applications. Since a SW CNT has dimensions comparable to typical biomolecules (e.g. DNA, whose width is approximately 2 nm), they should be capable of electrical sensing of single biomolecules [35]. A charged molecule near the SW CNT will act as an effective gate, changing the conductance of the tube. The large transconductances indicate that the signal from single molecules should be readily observable (Fig. 11).

C. Devices for Matching of Biosignal to Electronic Element (Circuit)

Creative integration of microchip technologies and nanostructures is feasible. By tuning the dielectrophoretic frequency within a microdevice, nanoparticles can be manipulated with the same precision as cells because a one-to-one correspondence exists between a given alternating current frequency and a nanoparticle interaction or biological event. Multiple biological events could be probed simultaneously provided that their corresponding frequencies are distinct. Combined with electroporation, electrokinetics also enables inclusion of molecular complexes inside the cells. Alternatively, functionalized nanoposts can be used to impale cells and relay information from the cell interior to nanoelectronic circuits. By merging the fields of microfluidics, electrokinetics, and cell biology, microchips are capable of creating tiny, mobile laboratories. The challenge for the future of designing a nano-interface in a microfluidic chip to probe a living cell lies in seamlessly integrating techniques into a robust and versatile, yet reliable, platform [36].

A planar FET can be configured as a sensor by modifying the gate oxide (without gate electrode) with molecular receptors or a selective membrane for the analyte of interest. Binding of a charged species then results in depletion or accumulation of carriers within the transistor structure. An attract-tive feature of such chemically sensitive FETs is that binding can be monitored by a direct change in conductance or related electrical property, although the sensitivity and potential for integration are limited. The so-called floating gate architecture combines a complementary metal oxide semiconductor (CMOS)-type n-channel FET with an independent sensing area for recording extracellular signals from electrogenic cells was presented [37]. This concept allows the transistor and sensing area to be optimised separately. The noise level of the devices was smaller than of comparable non-metallised gate FETs. The potential of NW nanosensors with direct, highly sensitive real-time detection of chemical and biological species in aqueous solution has been demonstrated [38]. A silicon NW (SiNW) solid state FET, whose conductance is modulated by an applied gate, is transformed into a pH nanosensor (Fig. 12) by modifying the silicon oxide surface with 3-aminopropyltriethoxysilane (APTES).

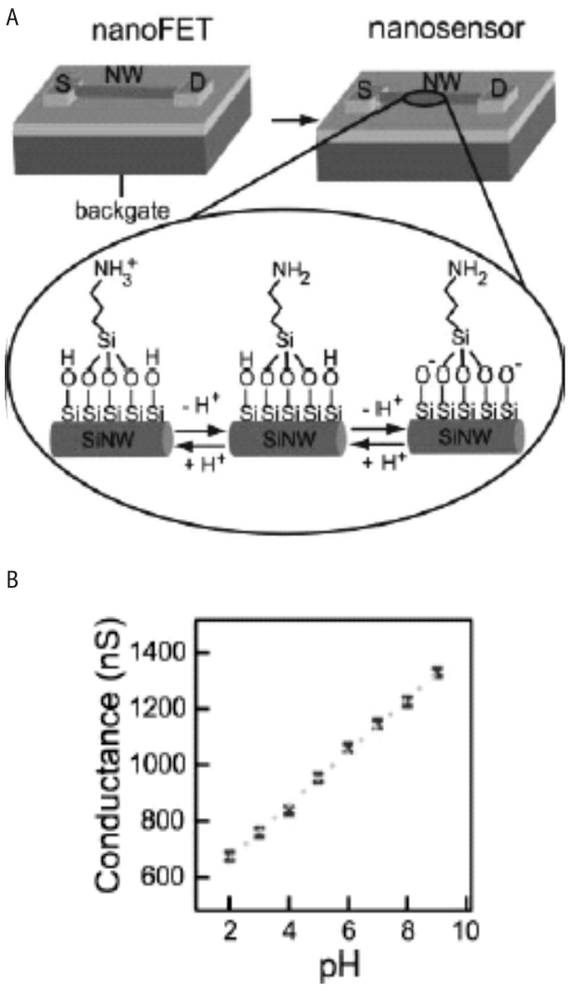

Fig. 12 A pH nanosensor
A - a silicon NW (SiNW) solid state FET;
B - measurements of conductance as a function of time and solution pH.

The report shows how the scientists fabricate FETs from CNT with the precise electrical properties and any variable band-gap desired. In parallel studies of CNT, researchers have been working to improve the electrical characteristics of individual nanotube transistors [39]

3. Microfluidic sensors of the biomechanical flows

The method of combining the bioelectric nature of MBs with body-temperature PC and zero resistance input of the SuFET device in order to obtain most advantageous biosensor/transducer was recently advanced [8]. The SuFET is used as a zero-resistance ammeter, which converts drain currents into gate voltages [40].

Microfluidic sensors promise detection of very low concentrations of analytes in volumes on the nanolitre scale [41]. A laser is integrated onto a microfluidic chip and investigated the device as a chemical detector.

A low intensity acoustic oscillation is used to create microfluidic domains whose chemical composition can be controlled electrochemically [42]. The acoustic oscillation impinges on a cylindrical object (an electrode), and the resulting time-averaged Reynolds stresses lead to a steady flow called acoustic streaming.

The practical absence of influence of the ultrasound oscillations on the flow's structure of controllable medium, the relative simplicity of introducing the oscillations, and processing of the acquired signals result in the extensive application of an ultrasound in the technique of measuring the flow rate of liquid and gaseous mediums [43]. During this process the speeds of expanding the oscillations in the non-moving medium and the speed of the medium itself are geometrically summationed. That is why it is necessary to introduce of receiving-transmitting devices into this medium.

The merits of laser flowratemeters are that they are non-contacting, have a high sensitivity, little inertia, wide range of measured speeds and flow rates, without being dependent on the physical properties of the investigating medium [44]. For this is necessary special-purpose windows in channel for getting through traverse of the laser beam. The new fiber-based optical microfluidic detectors, designed for nano-volume sample measurement, are known [5].

Another kind of flowratemeter-electromagnetic (EM) one-based on the law of EM induction-appearing a difference of potentials during moving of a conductor in MF [45]. A head sensor of the capacitive flowratemeters is based on changes of a capacitance during the contact of moving medium with plates [46]. These methods require action on the flowing medium, i.e. excitation by EM energy for the following reading of the gained effect out [47].

Taking into account the said considerations, it is necessary to lay down the fundamentals of non-contact passive FMs. It is based on the effect of creating the vortical MF by ionized particles of the substances. This MF is transduced into the measurable voltage by the torus-like pickup coil (PC) of the induction (search-coil) sensor/transducer (IS).

Non-contact passive measuring of the said substances and tissues is possible by using the induction sensor with solenoidal and/or toroidal pickup coil(s) (PC) which will embrace the flow [48]. These coil(s) can be both room-temperature and superconducting with connection to either common or superconducting FET. The measured quantities are: 1) vortical MF of gasiform stream for the toroidal PC, and 2) variation of the surrounding (natural) MF according to the magnetohydrodynamical (MGD) effect for the solenoidal PC.

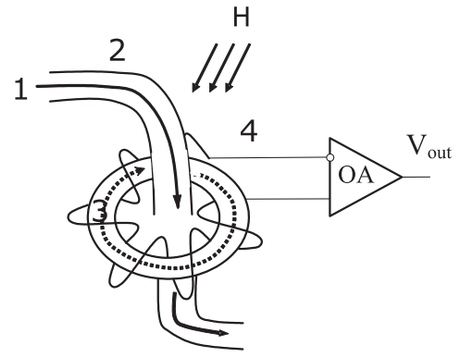

Fig. 13 The stream of gasiform or friable substances 1 through nonferromagnetic capillary 2 generating vortical MF H_{fi} 3 which is picked up by the room-temperature PC 4 of the ordinary or invented new superconducting transducer.

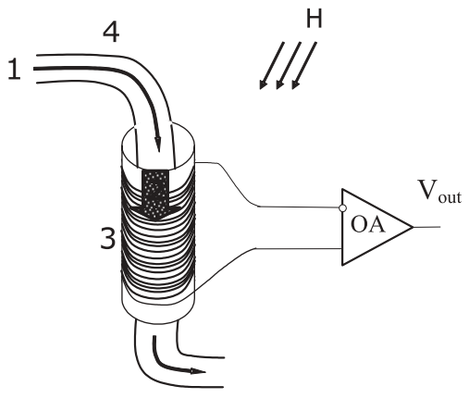

Fig. 14 The originated in the flow 1 partial H_{fi} 2 of the external natural MF H which picked up by solenoidal PC 3, which wrapped around the capillary 4, of the ordinary or superconducting transducer.

There are a variety of MF sensors/transducers including two passive ones of high sensitivity: IS and SQUID devices. Non-contact passive measuring of the said substances and tissues is possible by using only the IS with solenoidal and/or torus-like PCs which will embrace the flow. These coil(s) can be both room temperature and superconducting with connection to either common or superconducting FET. The said measured quantities are caused by the electrogaseodynamical jet or MGD flow. The invented transducer can be applied in FMs of gasiform and friable substances (Fig. 13) and liquid mediums (Fig. 14).

Measured MF interferes with the surrounding one. The variations of measured MF strength H_{fi} 1 of the stream (Fig. 13) or flow (Fig. 14) as a result of subtraction (Fig. 15):

$$H_{fi}=H_p-H_o, \quad (1)$$

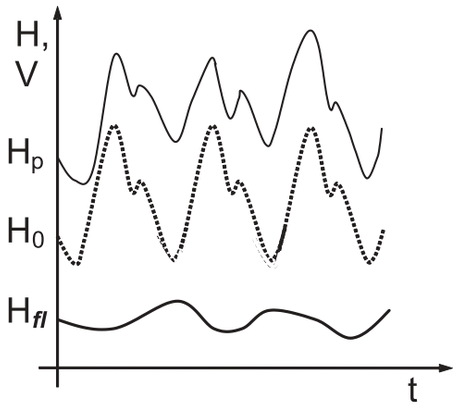

Fig. 15 A result of subtraction H_{fl} of the external natural MF H_0 from the field immediately around the capillary H_p.

which corresponds linearly to the difference of the respective output voltages of the transducer(s) as follows:

$$V_{fl}=V_p-V_o. \quad (2)$$

The method of measuring the volume flow of liquids and gaseous or friable substances by defining their interaction with only ambient natural MF. The first device based on this method is a passive and non-contact FM gase-ous or friable substances includes a resistive or superconducting torus-like PC of an IS which is PC-placed around the jet-flow. The second one is a FM of liquids and organic tissues (a blood) or a counter of the ferroma-gnetic particles into this mediums, consists of the same IS, but with a solenoidal-shape PC. As a result of such an arrangement, the head transducer is considerably simplified since it is the absence of the necessity of introducing any active interaction in the measured medium. The absence of mechanical interaction with flowing substances increases the reliability and life-span of the device. On the other hand, they completely retain the characteristics and composition of the flow compo-nents. Thus, the employment of a spontaneous MF causes the reduction of energy consumption to occur.

As a result of such arrangement, the measuring device is setting up without a failure of the capillaries and inter-rupting in their functioning. The absence of a measuring device or any moving members will considerably raise the safety factor in service due to the isolation of the flows from potentially combustible substances. It also, gives us the chance to avoid any influence on the measuring substance, including the danger of changing its chemical or physical composition.

A. Microfluidic Sensor of Gases

The profiles of microfluidic gas flow in capillaries and chip devices obtained by nuclear magnetic resonance (NMR) in the remote-detection modality was shown [49]. Through the transient measurement of dispersion, NMR is well adaptable for noninvasive yet sensitive determina-tion of the flow field and provides a potentially more powerful tool to profile flow in capillaries and miniatu-rized flow devices.

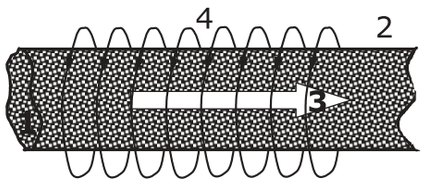

Fig. 16 The gasiform or friable substances 1 which ionized in consequence of interaction with the internal solid surface of capillary 2. The formed electrogaseodynamical jet 3 induce the vortical MF 4.

One of the main mechanisms of gases ionization is their interaction with the surface of the solid body, i.e. surface ionization [50]. Such interaction arouses an electrogaseodyna-mical flow [51] (Fig. 16):

$$I=/q_0u_0\pi h_i^2 \quad (3)$$

where:
q_0- the density of an electrical charge;
u_0- the dimensionless speed of a gas flow;
h_i- the radius of an electrogaseodynamical jet.

In such cases the MF strength (Fig. 16) on the distance r from the flow's edge is:

$$\Delta H=I/2\pi r \quad (4)$$

As a result we have an equation:

$$\Delta H=q_0u_0\pi h_i^2/2r \quad (5)$$

This flow is absorbed by the torus-like PC of an IS. It is necessary to notice, that an acquired value of MF strength will be generated outside the capillary only when it is made of parama-gnetic material. In the case of diamagnetical, and especially ferromagnetical metal or alloy, the measurement of some residual value occurs.

The performance of the microfluidic sensor of volume movement of these liquid substances and tissues laid down on measuring the variations of ambient MF strength will cause to pull it along with a moving medium which the strength crosses.

B. Microfluidic Sensor of Liquids

Because of low Reynolds numbers, laminar flow is usually assumed. However, either by design or unintentionally, the flow characteris-tic in small channels is often altered (e.g., by surface interactions, viscous and diffusional effects, or electrical potentials). Therefore, its prediction is not always straightforward. Currently, most microfluidic flow measurements rely on optical detection of markers, requiring the injection of tracers and transparent devices [49].

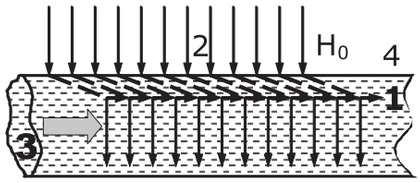

Fig. 17 The partial H_{fl} 1 of the external natural MF strength H_0 2 entrains by MGD flow 3 in the capillary 4.

Let us consider the MGD foundations of this phenomenon (Fig. 17). For the liquid that moves between two nonconducting walls in the direction of this motion the partial of the MF induction is arise:

$$B_x=B_0R_m\,\frac{sh(Mz/L_0)\ -\ (z/L_0)shM}{MchM\ -\ shM} \tag{6}$$

where
B_0 - the value of an ambient MF induction, which is perpendicular to the flow;
L_0 - a characteristic length;
Z- the centre of a flow, and $z=\pm L_0$ - the interval to the walls;
R_m- the magnetic Reynold's number;

and $$M=B_0L_0\sqrt{(\sigma/\rho\nu)}, \tag{7}$$

where
σ - a conductivity;
ρ - a density;
ν - the kinematic viscosity.
An equation for Rm is written down:

$$R_m=V_0L_0/\eta \tag{8}$$

where
V_0 - a characteristic velocity, which is comparable with an actual speed;

$\eta=1/\mu\sigma$ - the factor of MF diffusion; (9)

μ- the magnetic permeability (a medium is foreseen as nonmagnetic, $\mu=\mu0=4\pi\cdot10^{-7}$ henry/meter).

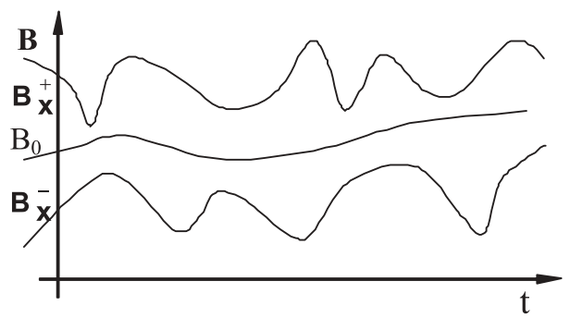

Fig. 18 A dynamical difference of an ambient MF changes between two places of capillary.

It is possible to count/register of the changes of the volumes by summation of the momentum, relative to B_0, values of B_x (MF strength) without having contact with them:

$$\Delta V_n=\frac{\sum_{i=1}^{n}(B_0\pm B_x^+)}{\sum_{i=1}^{n}(B_0\pm B_x^-)} \tag{10}$$

where opposite directions of the flows are defined by B_x^+ and B_x^-(Fig. 18).

Moreover, the gradiometrical configuration connection of PCs makes it possible to define the direction of the flow (B_0-B_x > 0 or < 0) and the dynamic nature of its' pulsations (B_0-B_x > or < B_0-B_x).

C. Counter of Ferromagnetic Particles

As we can notice, the value of in Eq.(8) should vary. That is why this variation will influence the measuring partial of MF: both B and strength H. It means that the variation of the density of ferro- or paramagnetic particles in(to) the stream can be determined when the speed of a stream is constant. To measure all three directions of blood velocity provides the ability to visualize two- or even three-directional blood flow patterns. It also promises a non-invasive quantification of the mechanical energy losses of blood as it flows through the connection. New rapid acquisition sequences show accuracy in quantifying flow [52].

Fig. 19 Variation H_{fl} of an ambient MF H in a BF secondary to the changes of ferrum molecules' density.

Let us proceed by explaining this technique using the example of the advancing counting/measuring device of hemoglobinum level in bloodflow (BF) [53]. This level is influenced by the paramagnetic susceptibility of the flow due to variation in the density of ferrum molecules into it. Such variations $\Delta H=H-H_{fl}$ in the ambient MF H are absorbed by a solenoidal PC which embraces the BF (Fig. 19). As a result the output voltage U_{out} of IS defines both the absolute value of hemoglobinum content and variations of it density in respect to some optimal value.

A hemoglobinum composition consists of a simple albumen- globin and a ferrum which consists of a non-albumen cluster- gem (96% and 4% in a ratio to the mass of molecule respectively). A gem is by itself protoporfin of ferrum- the combined compaund of protoporfin IX with twovalency ferrum [53].

The magnetic permeabillity of the medium (in this case BF) is defined as [54]:

$$\mu=1+\chi \tag{11}$$

The classical value of paramagnetic susceptibility derives as:

$$\chi_{cl}= \frac{NM_a^2}{3kT} \quad (12)$$

where
k- Boltzmann's constant;
T- absolute temperature.

Obviously that could be neglected by other chemical elements of gem with respect to M_a. Because in this case spontaneous magnetization is attributed only to ferrum molecules at the expense of a parallel orientation of spines (ferromagnetism).

In order to find a magnetic moment (MM) of ferrum in a gem composition, we can reference to for an analogy to a solid solution of a ferrum with silicon [55]. It is defined that this composition is ferromagnetic with MM for an atom of 2 mV, where $M_B=1.165\cdot10^{-29}$ (Wb·m) is a magneton of Bohr.

This give us the possibility of defining the magnetic susceptibility of blood according to a formula:

$$\mu=1+\chi_{cl}=1+\frac{NM_a^2}{3kT}=1+225\frac{NM_B^2}{kT} \quad (13)$$

By employing some substance as a core of PC is expected to define an effective magnetic permeabillity μ_{ef} of the formed physical body. As a big veines and arteries is possible to consider as a long cylinders, in consequence for them is valid an expression is [56]:

$$\mu_{ef}= \frac{\mu\mu_{dm}}{\mu+\mu_{dm}-1} \quad (14)$$

and

$$\mu_{dm}=m^2/(\ln 2m-1) \quad (15)$$

where m is a ratio of the length of a cylinder to the diameter.

As a result a formula for the PC's core which is formed by big BF vessels can be written down as:

$$\mu_{ef}= \frac{m^2(kT+225NM_B^2)}{m^2kT+225(\ln(2m)-1)NM_B^2} \quad (16)$$

An analysis of this formula provides evidence that requirement $\mu_{ef}>>1$ will be satisfied under condition $m^2>>\ln 2m-1$, which for long cores with m>>1 will always be true. That is why we acquire a ferromagnetic core in the form of a BF, which gives us the chance to create on its bases an IS from one of five modifications [57,58]. The input voltage of these ISs is defined by the known equations [57-60] and stand duty as measured quantity which is linearly connected with change μ_{ef} of PC, defined for a blood bed by Eq. (16).

The quantative content of hemoglobinum is defined by the difference between an IS's output voltages U_0- for a typical its value in some organism which is placed in the ambient permanent MF and Ux which has been measured for the investigated organism (Fig. 20). It is also possible to apply the external AC MF to a BF.

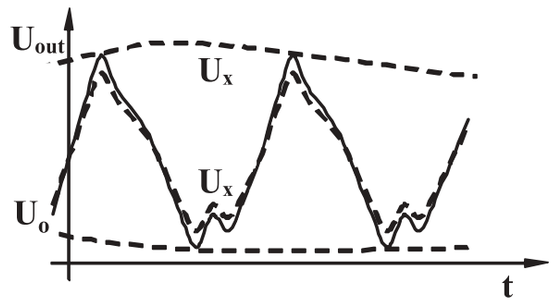

Fig. 20 A resulting voltage U_x of interference the magnetic component of a jet or flow with an ambient AC MF U_0.

In such cases a curve Ux establishes an envelope of AC signal which is modulated by BF dynamics.

4. The main arrangements of microfluidic sensors

Among the variety of the above presented FET devices there are majority of them, mainly modifications of nanoFETs, which allow simultaneous processing of a number of MBs directly or from the PC. There are two factors that make simultaneous processing possible. First of all, the sizes of nanoFETs and nanoPCs are in the same order as the transmitting substances of MBs, such as axons, neurons, and the DNA spiral. Secondly, the cNW-FET array (Fig. 7) is, in itself, multi-input.

The remaining part of FET devices are applicable for serial connection to the said mediums. In addition, some of these FETs can be arranged in the chain in order to transduce the MBs into different physical and chemical quantities and vice versa.

A. Serial Connection of MBs to the Microfluidic Sensor

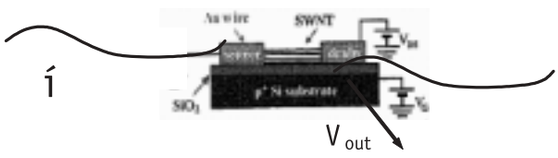

Fig. 21 Schematic of SuFETTr in the serial connection

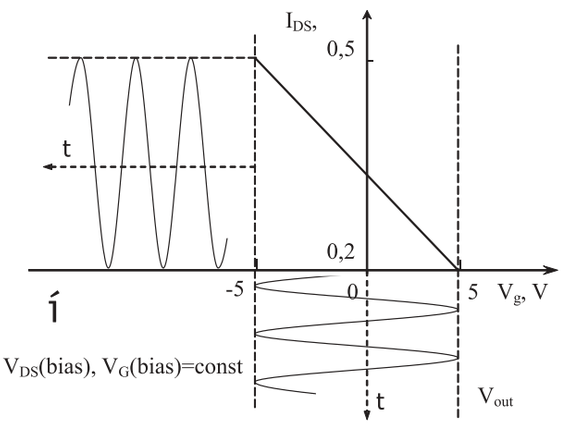

Fig. 22 Operational pattern of a serial SuFETTr

The organic or nanoSuFET device shown, for example in Fig. 9, is connected with the source of MBs through the said micro or nanocontacts according to Fig. 21. In such case the current of í, passing through the SuFET's channel arouses V_{out} on the gate with some constant bias voltages V_{DS}, V_G (Fig. 22). Transfer function (TF) of the device defined by its numerical order as follows:

$$K_{DNA}=\frac{V_{out}}{i}\Rightarrow\left[\frac{10}{0{,}5\mu A}\right]=2\cdot10^{7}\left[\frac{B}{A}\right] \quad (17)$$

As the channel of the majority of cited FETs is not superconducting in the present stage of development, it is possible to define the sensitivity threshold (ST) by the channel's resistance R:

$$U_{noise}^{DNA}=\sqrt{4kTR} \quad (18)$$

where
k - the Boltzmann constant,
T - absolute temperature of FET's channel.

The noise voltage of SuFETs is obtained analogous to the Johnson noise value for the resistive circuit as [40]:

$$(EN)^2=4kT_{SuFET}\gamma_{noise}/g_{dn} \text{ and } g_{dn}=I_0/V_c \quad (19)$$

where γ_{noise} is the ratio of the kinetic energy of the Josephson junction link to thermal energy and V_c - characteristic voltage. Ratio noise is proportional to the normalized gate charge g_G /C (g_G is the total gate charge reflected in the channel).

The peak currents range of MB from 5 to 10 μA [61] give a maximal output voltage V_{out} on absciss axis –5 to 5V also with the necessity of some its reducing it slightly by changing V_{DS}(bias) of the FET's channel. A current which elicits an action potential in the neuron is 0.6 nA [62] and will stimulate V_{out} of the transducer equal to 12 mV.

B. Parallel Connection of MBs to the Microfluidic Sensor

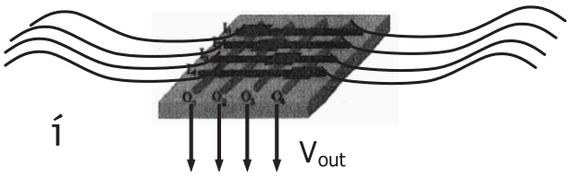

Fig. 23 Schematic of SuFETTr in the parallel connection

An example of connecting the axons of nerve fibre to multiinput cNW-FET [32] array is shown in Fig. 23. The output voltage of the transducer according to Fig. 8.B lies in the range of 1V (linear part of the curves).

The operational pattern of the transducer for one input MB into cNW-FET is shown in Fig. 21. The input MB changes conductance of the FET's channel which influences output voltage V_g.

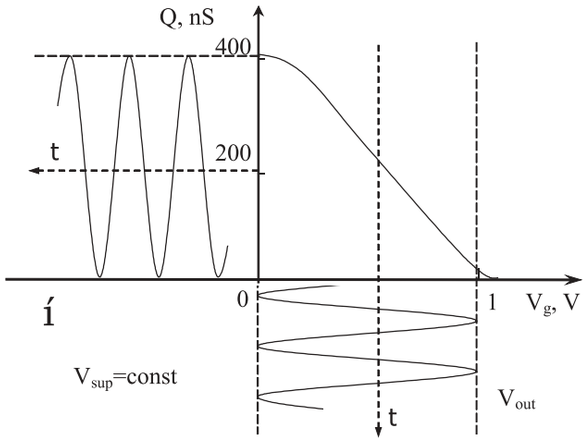

Fig. 24 Operational pattern of a parallel SuFETTr

TF of this device will be similar to the previous one:

$$K_{DNA}=\frac{V_{out}}{V_{sup}Q+i}\Rightarrow\left[\frac{1B}{10^{7}\,A}\right]\cong10^{7}\left[\frac{B}{A}\right] \quad (20)$$

Similarly the value of V_{out} can be obtained for organic, chemical and DNA microfluidic sensors.

The carrier density thus obtained is a function of the distance x from the interface (Fig. 3). The large carrier density at V_G=0V in small x region is due to the charge transfer from the Au electrodes to the pentacene molecules [3]. Carrier density n(x) is a function of the distance (x) from the interface at various gate voltages (V_G). According to the Eq.(4) deviation of carrier density n(x) in the range of maximal V_{out}=±15V is equal to $(7\div0)\cdot10^{17}/cm^3$.

Chemical microfluidic sensor converts the changes in pH through Q of the channel (similarly to pH nanosensor Fig. 12,A [38]) also into output signal V_{out}. In the scale of Q from 10 to 400 nS a pH (2 to 10) is transformed into variations of V_{out} from 0 to 1V (Fig. 27).

The potential applied during immobilisation of thiol-modified DNA lies in a different potential window from -0.7V to +0.7V [2]. The corresponding current í=V_{in}Q, to this voltage which is put into the FET channel, according to Fig. 24 vary from 0.4 to 1.8 nA.

Clean gold monolayers are stable in the potential range from -400 to +1400mV in dilute sulfuric acid solutions, thus allowing electrochemical applications. The careful selection of the terminal functionalities of the monolayers and the proper surface chemistry allows a tremendous flexibility in biosensor design.

ST of the biosensor/transducer in the first approximation (generally) depends on the conductance Q of the superconducting channel. An absolute sensitivity of the transducer with n parallel inputs in the said frequency range derives also from the Johnson noise:

$$U_{noise}^{DNA}=\sqrt{4kTR} \quad (21)$$

which for cNW-FET varies in the range 50 to 150 nS [32] and gives the order of ST 10^{-7} V/√Hz. Also for the noise voltage of parallel SuFETs based transducer is:

$$(E_N)^2(n)=4nkT_{SuFET}\gamma_{noise}/g_{dn} \quad (22)$$

5. Results

Application variety of the novel superconducting, organic and CNT FETs allows us to design transducers of MBs (ionic, nerve, DNA, etc.) that transduce them into different quantities, including electric voltage, density of chemical and biomolecules. On the other hand, the said MBs can be controlled by the applied electrical signals, or bio and chemical mediums.

Table 1. Dependence of the received MB parameters on the mode of microfluidic sensor's functioning

Mode / Medium	Serial		Parallel	
	external	implantable	external	implantable
Current	∫i-1 cont. or sens. imp.	$i=i(f_1)+i(f_2)+...+i(f_N)$	di/dt, di/dx	∑i=1 network or 1 fibre
Molecules	∫ECs→bio and chem. molec.	variation of ECs→ concentr. 4of molec.	∑ECs=1 type of molec.	∑ECs=∑ bio and chem. molec.
DNA	propagation of BS along DNA's spirals	decoding the BSs of nucleoted recognition	space and lengh dynamic on both spirals	4 nucleoteds→ 4 outputs

The described microfluidic sensors designed on the basis of organic and nano SuFETs are suitable for describing the wide range of MB dynamical parameters (see Table 1). Following the columns of the table, it should be noticeable, that serial connection of the external PCs allows us to gain some integrated signal, i.e., the whole sensing or control currents, which spreads along the number of axons of the nerve fibre; the amount of ions passing through the PCs and the generalized MB passing through one or both spirals of DNA. When SuFET channel(s) of are implanted into the tissue or process we can acquire more precise data about the frequency distribution of currents, volume distribution of ionized molecules and detecting activity of individual nucleoteds.

Exploitation of the parallel input to SuFETTr allows determination of space and time dynamics of MBs in the nerve fibre and DNA spiral(s) and also the amplification of output signal U_{out} by multiplying the concentration of molecules according to a number of input MBs. After the implantation of parallel SuFET(s), the averaging or summation of this dynamic among the whole flow network, nerve fibre or DNA spiral(s) is possible.

6. Conclusion

The invented microfluidic Sensor has the following fundamental improvements upon existing ones:

a) the sign of the output voltage permits the determination of the direction of the input bioflow passing through a single SuFET device;
b) the capability to regulate the proportion of axons, neurons or flows that are being investigated to the untouched ones- either the whole cross section of the fibre or flow, or any part of them;
c) the possibility to substitute the SuFET device or to adjust its ratings to comply with the conditions of the measurement process without repeatedly destroying nerve fibre or flow vessel;
d) the transducer could create conversion in both directions, respectively in passive and active modes;
e) the combination of biocompatibility and tissue equivalence in both the diamond and protein-based (organic) FETs makes them naturally fit for implantation.

The reviewed variety of FETs shows the varying extent of readiness for them to be exploited them in microfluidic Sensor of MBs. The most appropriate for such an application are the ordinary solid-state SuFET modifications and novel CNT based SuFETs. The organic SuFETs are not amply developed, but this work is being carried out in a number of directions. At the same time, the PCs, which are necessary for the external sensor with respect to the transducing medium (solid-state conductor, nerve fibre, flow of ions and DNA spiral), and corresponding low-ohmic wire traces for connecting PCs to the FET's channel are sufficiently developed, even at nano dimensions.

The preliminary calculations confirm the possibility of broadening the microfluidic sensors' action from MF to the biochemical medium of MBs. The main parameters of such MBs can be gained by applying the arrangement of the microfluidic sensors to the whole measurement system. Two directions of microfluidic sensor function enable decoding of the MB by comparing the result of its action on some process or organ with an action on them of the simulated electrical or biochemical signal after their reverse transducing through the microfluidic sensors. Furthermore, this decoded signal will provide a basis for creating feedback and feedforward loops in the measuring system for more precise and complete influence on the biochemical process.

AUTHOR
Rostyslav Sklyar – Space Sensing Instruments, Verchratskogo st. 15-1, Lviv 79010 UKRAINE; tel./fax: +380 322 762432/769613, e-mail: sr@tiar.net.

References

[1] Weiss H., "Electrical measurement and instrumentations - today and tomorrow", *Measurement*, 1993, no. 12, pp. 191-210.

[2] Lucarelli F., Marrazza G., Turner A. P. F. et al., "Carbon and gold electrodes as electrochemical transducers for DNA hybridisation sensors" (Review), *Biosensors and Bioelectronics*, 2004, no. 19, pp. 515-530.

[3] Kiguchi M., Nakayama M., Fujiwara K. et al., "Accumulation and Depletion Layer Thick-nesses in Organic Field Effect Transistors", *Jpn. J. Appl. Phys.*, vol. 42, 2003, no. 2, L1408-L141.

[4] Fromherz P., Vassanelli S., and Greeff N. G., *NACHIP Project*, Reference: IST-2001-38915. Available at: http://www.biochem.mpg.de/mnphys/europroject/project.html (2006).

[5] Bargiel S., Górecka-Drzazga A., Dziubana J. A. et al., "Nanoliter detectors for flow systems", *Sens. Act.* A, 2004, no. 115, pp. 245-251.

[6] Stroscio M. A., Dutta M., "Integrated biological-semiconductor devices", *Proc. IEEE 93*, 2005, pp. 1772-1783.

[7] Helmke B. P., Minerick A. R., "Designing a nano-interface in a microfluidic chip to probe living cells: Challenges and perspectives", *PNAS, 2006*, no. 103, pp. 6419-6424.

[8] Sklyar R., "A SuFET Based Either Implantable or Non-Invasive (Bio)Transducer of Nerve Impulses", *13th International Symposium on Measurement and Control in Robotics - ISMCR'03*, Madrid, Spain 2003, pp. 121-126.

[9] Cheunga K. C., Renaudb Ph., "BioMEMS for medicine: On-chip cell characterization and implantable microelectrodes", *Solid-State Electronics*, 2006, no. 50, pp. 551-557.

[10] Kanoun O., Tränkler H.-R., "Sensor Technology Advances and Future Trends", *IEEE Trans. Instrum. Meas.*, 2004, no. 53, pp. 1497-1501.

[11] Lutz B. R., Chen J., and Schwartz D. T., "Microfluidics without microfabrication", *PNAS, 2003*, no. 10, pp. 4395-4398.

[12] Shaikh K. A., Ryu K. S., Goluch E. D., et al., "A modular microfluidic architecture for integrated biochemical analysis", *PNAS, 2005*, no. 102, pp. 9745-9750.

[13] Sinha N., Yeow J. T.-W., "Carbon Nanotubes for Biomedical Applications", *IEEE Trans. Nanobiosc.*, 2005, no. 4, pp. 180-195.

[14] Hopkins D. S., Pekker D., Goldbart P. M., et al., "Quantum Interference Device Made by DNA Templating of Superconducting Nanowires", *Science*, 2005, no. 308, pp. 1762-1765.

[15] Gross M., Altpeter D., Stieglitz T. et al., "Micromachining of flexible neural implants with low- ohmic wire traces using electroplating", *Sens. Act.* A, 2002, no. 96, pp. 105-110.

[16] K. C. Cheunga, Ph. Renaudb, "BioMEMS for medicine: on-chip cell characterization and implantable microelectrodes", *Solid-State Electronics*, 2006, no. 50, pp. 551-557.

[17] E. Arzt, S. Gorb, and R. Spolenak, "From micro to nano contacts in biological attachment devices", *PNAS*, 2003, vol. 100, pp. 10603-10606.

[18] R. G. Ellis-Behnke, Y.-X. Liang, S.-W. You et al., "Nano neuro knitting: peptide nanofiber scaffold for brain repair and axon regeneration with functional return of vision", *PNAS*, 2006, vol. 103, pp. 5054-5059.

[19] A. V. Liopo, M. P. Stewart, J. Hudson et al., Biocompatibility of native and functionalized single-walled carbon nanotubes for neuronal interface, *J. Nanosci. Nanotechnol,* 2006, no. 6, pp. 1365-1374.

[20] J. Thomas, "Nanowires: Domain walls", Nature Nanotechnology, (Published online: 8 December 2006 at: www.nature.com/nnano/reshigh/2006/1206//full/nnano.2006.186.html [doi:10.1038/nnano.2006.186].

[21] F. S. Ou, M. M. Shaijumon, L. Ci et al., "Multisegmented one-dimensional hybrid structures of carbon nanotubes and metal nanowires", *Appl. Phys. Lett.*, 2006, no. 89, 243122 (3 pages).

[22] J. F. Jiang, Q. Y. Cai, H. M. Jiang et al., "High-performance complementary metal-oxide-superconductor field effect transistor (CMOSuFET) current-mode operational amplifier", *Supercond. Sci. Technol.*, 1996, no. 9, pp. A66-A70.

[23] Sh. Suzuki, H. Tobisaka, and Sh. Oda, "Electric properties of coplanar high-Tc superconducting field-effect devices", *Jpn. J. Appl. Phys.*, vol. 37, 1998, Pt. 1, pp. 492-495.

[24] B. Yu, M. Meyyappan, "Nanotechnology: role in emerging nanoelectronics", *Solid-State Electronics*, 2006, no. 50, pp. 536-544.

[25] J. H. Schön, Ch. Kloc, and B. Batlogg, "High-temperture superconductivity in lattice-expanded C_{60}", *Science*, 2001, no. 293, pp. 2432-2434.

[26] J. H. Schön, H. Meng, and Z. Bao, "Field-effect modulation of the conductance of single molecules", *Science*, 2001, no. 294, pp. 2138-2141.

[27] K. Nakamura, M. Ichikawa, R. Fushiki et al., "Organic field-effect transistor of (thiophene/phenylene) co-oligomer single crystals with bottom-contact configuration", *Jpn. J. Appl. Phys.*, 2004, no. 43, L100-L102.

[28] T. Jung, B. Yoo, L. Wang et al., "Nanoscale n-channel and ambipolar organic field-effect transistors", *Appl. Phys. Lett.*, 2006, no. 88, 183102 (3 pages).

[29] J. A. Garrido, C. E. Nebel, and R. Todt, "Fabrication of in-plane gate transistors on hydrogenated diamond surfaces", *Appl. Phys. Lett.*, 2003, no. 82, pp. 988-1000.

[30] P. Avouris, J. Appenzeller, R. Martel et al., Carbon nanotube electronics, *Proc. of the IEEE*, 2003, pp. 1772-1784.

[31] F. Nihey, H. Hongo, Y. Ochiai et al., "Carbon-nanotube field-effect transistors with very high intrinsic transconductance", *Jpn. J. Appl. Phys.*, 2003, Pt. 2, no. 42, L1288-L1291.

[32] Z. Zhong, D. Warmg, and Y. Cui, "Nanowire crossbar arrays as address decoders for integrated nanosystems", *Science*, 2003, no. 302, 1377-1379.

[33] K. Keren, R. Berman, E. Buchstab et al., "DNA-templated carbon nanotube field-effect transistor", *Science*, 2003, no. 302, pp. 1380-1382.

[34] G. Stix, "Nano Patterning", *Scientific American*, February 2004.

[35] S. Rosenblatt, Y. Yaish, J. Park et al., "High performance electrolyte gated carbon nanotube transistors", *Nano Lett.*, 2002, no. 2, pp. 869-872.

[36] B. P. Helmke, A. R. Minerick, "Designing a nano-interface in a microfluidic chip to probe living cells: Challenges and perspectives", *PNAS*, 2006, vol. 103, pp. 6419-6424.

[37] S. Meyburga, M. Goryllb, J. Moersb et al., "N-channel field-effect transistors with floating gates for extracellular recordings", *Biosens. Bioelectr.*, 2006, no. 21, pp. 1037-1044.

[38] Y. Cui, Q. Wei, H. Park et al., "Nanowire Nanosensors for Highly Sensitive and Selective Detection of Biological and Chemical Species", *Science*, 2001, no. 293, pp. 1289-1292.

[39] Ph. G. Collins, M. S. Arnold, and Ph. Avouris, "Engineering carbon nanotubes and nanotube circuits using electrical breakdown", *Science*, 2001, no. 292, pp. 706-709.

[40] R. Sklyar, "Superconducting Induction Magnetometer", *IEEE Sensors J.*, 2006, no. 6, pp. 357- 364.

[41] D. Gevaux, "Microfluidics: Feel the flow", *Nature Photonics* (Published online: 7 December 2006 at: www.nature.com/nphoton/archive[doi:10.1038/nphoton.2006.71].

[42] B. R. Lutz, J. Chen, and D. T. Schwartz, "Microfluidics without microfabrication", *PNAS*, 2003, vol. 100, pp. 4395-4398.

[43] A. Sh. Kilsbeyli, A. M. Izmailov, V. M. Gurevich, "The Frequency-Time Ultrasound Flowratemeters and Counters", *Mashynostroenie*, 1984, Moscow.

[44] B. G. Ceytlin, *The Technics of Measuring the Flow Rate and Quantity of Liquids, Gases and Vapors,* Publishing of Standarts, Moscow, 1981.

[45] M. F. Feller, *Patent* US 4535637 (1985).

[46] R. G. Green, *Patent* GB 2147106 (1985).

[47] J. Knaak, *Patent* EP 0149771 (1985).

[48] R. Sklyar, *Patent* UA No65546, Ukrainian State Patent Office (2004), Bulletin No 4.

[49] Ch. Hilty, E. E. McDonnell, J. Granwehr et al., "Microfluidic gas-flow profiling using remote-detection NMR", *PNAS,* 2–5, vol. 102, pp. 14960-14963.

[50] *Physical Encyclopedy*, Moscow 2 (1990).

[51] A. B. Vatazhyn, *The Electrogaseodynamical Flows*, Moscow: Nauka, 1989.

[52] G. P. Chatzimavroudis, "Blood Flow Measurements With Magnetic Resonance Phase Velocity Mapping", Measurement , 2005, no. 37, pp. 201-212.

[53] *A Big Medical Encyclopedy*, Moscow 5 (1975).

[54] M. I. Kaganov, V. M. Tsukernic, *A Nature of Magnetism*, Library of "Kvant", Moscow 16, 1982.

[55] S. Takadzumi, *Physics of a ferromagnetism. The magnetic characteristics of a material*, Moscow: Mir, 1983.

[56] K. Hayashi, T. Oguti, T. Watanabe, "Absolute Sensitivity of a High- Metal Core Solenoid as a Magnetic Sensor", *J. Geomag. Geoelectr.*, 1978, no. 30, pp. 619-630.

[57] I. M. Hontar, L. YA. Mizyuk, R. V. Protz, "Wide band induction transducers of magnetic field strength with stable sensitivity in a frequency range", *Otbor e obrabotka informatsee* (in Rus.), 1983, no. 68, pp. 74-80.

[58] R. Sklyar, *Patent* UA No21185, Ukrainian State Patent Office (2000), Bulletin No1.

[59] L. F. Zambresky, T. Watanabe, "Equivalent Circuit of a Magnetic Sensor Coil and a Simple Filter for Rejection of 60 Hz Man- Made Noise", *J.Geomag. Geoelectr.*, 1980, no. 32, pp. 325-331.

[60] K.-P. Estola, J. Malmivuo, "Air-Core Induction Coil Magnetometer Design", *J. Phys. E: Sci. Instrum.*, 1982, no. 15, pp. 1110-1113.

[61] M. Jenkner, B. Muller, and P. Fromherz, "Interfacing a silicon chip to pairs of snail neurons connected by electrical synapses", *Biol. Cybern.*, 2001, no. 84, pp. 239-249.

[62] J. P. Wikswo, J. P. Barach, and J.A. Freeman, "Magnetic Field of a Nerve Impulse: First Measurements", *Science*, 1980, no. 208, pp. 53-55.